Modeling soil metabolic processes using isotopologue pairs of position-specific ^{13}C-labeled glucose and pyruvate

Paul Dijkstra [a,*], Jacob J. Dalder [a], Paul C. Selmants [b], Stephen C. Hart [c,d], George W. Koch [a,e], Egbert Schwartz [a], Bruce A. Hungate [a,e]

[a] Department of Biological Sciences, Northern Arizona University, P.O. Box 5640, Flagstaff, AZ 86011, USA
[b] Environmental Studies Department, University of California, Santa Cruz, CA 95064, USA
[c] School of Natural Sciences, University of California, Merced, CA 95343, USA
[d] Sierra Nevada Research Institute, University of California, Merced, CA 95343, USA
[e] Merriam-Powell Center for Environmental Research, Northern Arizona University, P.O. Box 5640, Flagstaff, AZ 86011, USA

ARTICLE INFO

ABSTRACT

Most organic carbon (C) in soils eventually turns into CO_2 after passing through microbial metabolic pathways, while providing cells with energy and biosynthetic precursors. Therefore, detailed insight into these metabolic processes may help elucidate mechanisms of soil C cycling processes. Here, we describe a modeling approach to quantify the C flux through metabolic pathways by adding 1-^{13}C and 2,3-^{13}C pyruvate and 1-^{13}C and U-^{13}C glucose as metabolic tracers to intact soil microbial communities. The model calculates, assuming steady-state conditions and glucose as the only substrate, the reaction rates through glycolysis, Krebs cycle, pentose phosphate pathway, anaplerotic activity through pyruvate carboxylase, and various biosynthesis reactions. The model assumes a known and constant microbial proportional precursor demand, estimated from literature data. The model is parameterized with experimentally determined ratios of $^{13}CO_2$ production from pyruvate and glucose isotopologue pairs. Model sensitivity analysis shows that metabolic flux patterns are especially responsive to changes in experimentally determined $^{13}CO_2$ ratios from pyruvate and glucose. Calculated fluxes are far less sensitive to assumptions concerning microbial chemical and community composition. The calculated metabolic flux pattern for a young volcanic soil indicates significant pentose phosphate pathway activity in excess of pentose precursor demand and significant anaplerotic activity. These C flux patterns can be used to calculate C use efficiency, energy production and consumption for growth and maintenance purposes, substrate consumption, nitrogen demand, oxygen consumption, and microbial C isotope composition. The metabolic labeling and modeling methods may improve our ability to study the biochemistry and ecophysiology of intact and undisturbed soil microbial communities.

© 2011 Elsevier Ltd. All rights reserved.

1. Introduction

Most plant-derived carbon (C) is lost as CO_2 or ends up as stable soil organic matter after passing through microbial metabolic pathways. Heterotrophic soil microbes utilize organic-C substrates for energy production and biosynthesis. The partitioning of substrate between energy production and biosynthesis (C Use Efficiency − CUE) has consequences for soil respiration and soil C storage (Allison et al., 2010; Davidson and Janssens, 2006; Manzoni and Porporato, 2009; Six et al., 2006), but is difficult to determine in the spatially and temporally complex environment of soils (Frey et al., 2001; Herron et al., 2009; Thiet et al., 2006). Here, we present a new approach to determine aspects of energy production, biosynthesis, CUE, and biochemical regulation of C transformations using a model of soil microbial metabolic processes. This paper combines the technique of position-specific ^{13}C-labeled metabolic tracer labeling (Dijkstra et al., 2011) with a metabolic model of C processes. This model can be further developed, experimentally tested, and used to elucidate relationships between microbial ecophysiology and C cycling processes in soils.

In a previous paper, we used parallel incubations of soil amended with small amounts of position-specific ^{13}C-labeled pyruvate to evaluate the relative activity of glycolysis and Krebs cycle in soil

* Corresponding author. Tel.: +1 928 523 0432.
E-mail address: paul.dijkstra@nau.edu (P. Dijkstra).

microbial communities (Dijkstra et al., 2011). However, because of the complexity of the metabolic system, it is essential to use models to achieve a quantitative interpretation of these results. Metabolic networks are routinely modeled for industrially important microbial species and increasingly used to study biochemistry and physiology in plant and animal species (e.g., Fernie et al., 2005; Kruger and Ratcliffe, 2009; Stephanopoulos, 1999; Wiechert et al., 2001; Zamboni and Sauer, 2009). These models determine the probabilistic path of each C atom from substrate molecules into microbial products, such as amino acids, lipids, and CO_2. The partitioning of pyruvate-C (and other metabolic tracers) between microbial products and CO_2 is determined by the pattern of C flux through the metabolic network, which is a function of microbial demand for energy and biosynthesis, available substrates, and environmental conditions.

A simple example illustrates the principle of these model calculations: when substrate is used for the production of energy but not for biosynthesis, C from all positions will be released as CO_2 in the same proportion as present in the substrate. However, when biosynthesis is active, some C atoms have a higher probability to end up in biosynthesis products, while others are more likely to be released as CO_2. Carbon in position 1 (C_1) of pyruvate, glycine and alanine are released as CO_2 to a greater degree than C in positions 2 and 3 ($C_{2,3}$; Dijkstra et al., 2011; Fischer and Kuzyakov, 2010; Kuzyakov, 1997; Näsholm et al., 2001). From the differences in $^{13}CO_2$ production of two position-specific ^{13}C-labeled metabolic tracer isotopologue pairs, we can model the reactions of the C metabolic network.

The model described in this paper, derived from more complex models (Quek et al., 2009; Suthers et al., 2007; Yang et al., 2005), consists of three parts. The stoichiometric model describes net C fluxes through metabolic pathways (Fig. 1, Appendix Table 1). The atom mapping matrices (Zupke and Stephanopoulos, 1994) describe how individual C atoms change position from substrate to product for each reaction. Finally, the label identification vector is

a vector for each reaction that identifies which C atoms are ^{13}C labeled. The model calculates the steady-state $^{13}CO_2$ production from various position-specific ^{13}C-labeled metabolic tracer isotopologues for a given C flux pattern. These modeled results are then matched to experimentally determined $^{13}CO_2$ production ratios of the same metabolic tracers.

The use of position-specific ^{13}C-labeled tracers in soil is complicated by the presence of mineral and organic surfaces onto which these compounds may sorb. For this reason, each metabolic tracer is represented by a pair of isotopomers or isotopologues. By calculating the ratio of $^{13}CO_2$ production from two isotopologues of the same metabolic tracer, effects of sorption and incomplete uptake by microbial cells are canceled out, as both isotopologues will be equally affected by these processes (Dijkstra et al., 2011). In this paper, we demonstrate how combining two metabolic tracers, glucose and pyruvate, each represented by a pair of isotopologues, can be used to model the microbial metabolic system for a microbial community in young volcanic soil (Selmants and Hart, 2008, 2010).

2. Materials and methods

2.1. Experimental procedures

Soil (0−10 cm depth, A-horizon; Typic Ustorthent) was collected within a 5-m^2 plot in piñon-juniper woodland on 19 and 29 July 2010 at a site near Sunset Crater (1905 m above sea level, 111° 25′ 26″ W; Flagstaff, AZ; MAT = 11 °C, MAP = 340 mm y^{-1}). Soil was developed from basaltic cinder deposited 930 y ago (Selmants and Hart, 2008, 2010). Soil δ^{13}C value was −23.6‰, while soil total C concentration was 0.8% and soil total N concentration was 0.044%. Gravimetric soil moisture content was between 2 and 4% on 19 July and 7 and 8% on 29 July 2010.

Soil was sieved (2 mm mesh) and stored for at most four days at 4 °C in the dark. Once a day, 50 g aliquots were weighed into five
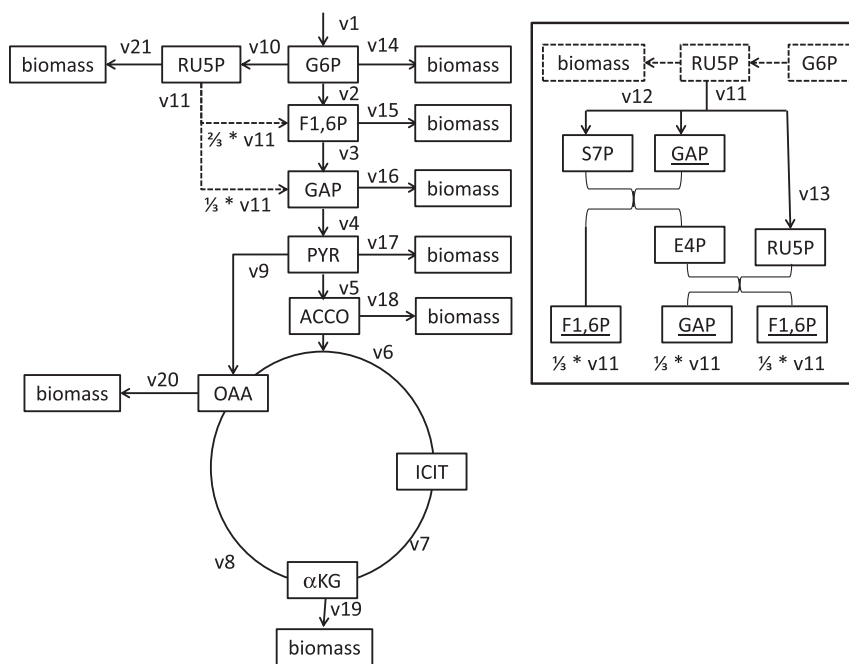
Fig. 1. A simple model for metabolic processes in soil microbial communities. Flux rates (v_2–v_{21}) are normalized to glucose uptake rate (v_1, set at 100) on a molar basis. Pentose phosphate pathway details are given in a separate box. Abbreviations: G6P, glucose-6P; F1,6P, fructose-1,6P_2; GAP, glyceraldehyde-P; PYR, pyruvate; ACCO, acetyl-CoA; ICIT, iso-citrate; αKG, α-ketoglutarate; OAA, oxaloacetate; RU5P, ribulose-5P; S7P, sedoheptulose-7P; E4P, erythrose-4P. See also Appendix Table 1.

specimen cups, soil moisture content adjusted to field capacity (determined according to Haubensak et al., 2002), and incubated overnight in airtight Mason jars (473 ml volume; Jarden Company, Rye, NY, USA) at 20 °C in the dark. Soils were treated with metabolic tracers the next day. These five aliquots formed one experimental replicate. Since we could analyze only one replicate per day, we repeated this process eight times. To minimize any effects of soil storage, we collected new soil from the same location after the first four replicates. Any effects of soil storage and sampling date were included in the experimental error.

Eighteen hours after start of the incubation, jars were opened and headspace was refreshed. After closing, 10 ml of pure CO_2 ($\delta^{13}C = -6.8‰$) was added to the headspace and isotope composition of CO_2 in each jar was determined 30 min thereafter by sampling 10 ml of headspace atmosphere. The 10 ml headspace sample was injected into a Tedlar air-sample bag (Zefon International, Ocala, FL, USA) and qualitatively diluted with CO_2-free air. The initial injection with pure CO_2 was carried out to satisfy the requirement of the Picarro G1101-*i* CO_2 cavity ring-down isotope spectrometer (Picarro Inc., Sunnyvale, CA, USA) for a CO_2 concentration between 300 and 2000 $\mu mol\ mol^{-1}$, while subsequent dilution with CO_2-free air was done to generate enough volume to enable 10 min analysis per sample. We determined the CO_2 concentration of the initial headspace atmosphere using a LICOR 6262 (Licor Inc., Lincoln, NE, USA).

Following the initial headspace measurement, 2 ml of a 3.6 mmol l^{-1} position-specific 1-^{13}C or 2,3-^{13}C-labeled sodium pyruvate solution or 2 ml of a 1.8 mmol l^{-1} 1-^{13}C or U-^{13}C glucose solution was injected through a septum onto the surface of the soil. Control soil received a similar amount of unlabeled glucose (first four replicates) or pyruvate (second four replicates). Pyruvate and glucose isotopologues were 99 atom% ^{13}C-enriched at the indicated C positions (Cambridge Isotope Laboratories, Andover, MA, USA). All jars received 0.43 μmol tracer-C per g soil. Isotope composition of CO_2 was determined 10, 20, 40, 60, and 120 min after tracer addition. The $^{13}CO_2$ production from metabolic tracers was calculated from the $^{13}CO_2$ produced from the soil with metabolic tracer corrected for $^{13}CO_2$ produced from control soil. Jars were not opened between measurements.

We calculated the ratios of position-specific $^{13}CO_2$ production from the two isotopologues for each metabolic tracer, as

$$C_1/C_{2,3} \text{ ratio} = \frac{^{13}CO_2 \text{ production from } 1 - {}^{13}C \text{ pyruvate}}{^{13}CO_2 \text{ production from } 2,3 - {}^{13}C \text{ pyruvate}}. \quad (1)$$

Similarly,

$$C_U/C_1 \text{ ratio} = \frac{^{13}CO_2 \text{ production from } U - {}^{13}C \text{ glucose}}{^{13}CO_2 \text{ production from } 1 - {}^{13}C \text{ glucose}}. \quad (2)$$

Soil respiration rates were determined separately on soil in Mason jars without CO_2 injection. Jars were opened and headspace atmosphere was refreshed. Two hours later, an initial headspace sample was analyzed for CO_2 concentration with the LICOR 6262. This measurement was repeated 24 h later.

2.2. Modeling metabolic flux networks

The metabolic model used to determine C flux patterns over the various biochemical pathways consisted of three interacting parts: a stoichiometric model that contained all the C transformations in the network, atom mapping matrices that described how C atoms change from product to substrates in each reaction, and a label identification vector that contained information on which C atoms were ^{13}C labeled. The three model elements together predict where

specific ^{13}C-labeled C atoms from metabolic tracers are released as CO_2 or incorporated into biomass.

2.2.1. Stoichiometric model

The stoichiometric network (Fig. 1, Appendix Table 1 for model equations), constructed in Excel, described the steady-state partitioning of glucose across the reactions of glycolysis, pentose phosphate pathway, and Krebs cycle. Pyruvate carboxylase was considered the main anaplerotic reaction (v_9), balancing the consumption of precursors from Krebs cycle pools for the purpose of biosynthesis (v_{19}, v_{20}). The pentose phosphate pathway produced pentoses for nucleotide synthesis, but also allowed C to flow back to glycolysis. This metabolic pathway helped satisfy the cell's demand for NADPH. Several reactions and metabolite pools were lumped, for example dihydroxyacetone-P, glyceraldehyde-P, phosphoglycerate, and phosphoenolpyruvate with glyceraldehyde-P. Fluxes ($v_1 - v_{21}$) were assumed to be greater or equal to zero (in the direction of the arrows). Pool sizes were considered small relative to flux rates. Fluxes going into and out of metabolite pools added up to zero (to meet the assumption of steady state for metabolite pools; this assumption was not made for the much larger biomass pools). The reaction network included eight biomass reactions ($v_{14} - v_{21}$). Carbon dioxide was produced by 6-phosphogluconate dehydrogenase, pyruvate dehydrogenase, isocitrate dehydrogenase and α-ketoglutarate dehydrogenase, the dominant decarboxylating reactions, while that from other processes such as amino acid synthesis was ignored. Carbon dioxide used in the anaplerotic reaction was assumed to be unlabeled. We also assumed that glucose was the only C substrate utilized by microbial cells. This metabolic model consisted of 21 reactions (including the reactions of the pentose phosphate pathway − Fig. 1). The reactions of the non-oxidative branch of the pentose phosphate pathway were fully dependent on v_{11} (Fig. 1 insert), reducing the model to 19 variables. Each node generates one equation assuming input equals output. This creates a set of 9 equations with 19 unknowns. To solve these equations, we estimated values for 10 unknown variables. By expressing all rates relative to v_1 (glucose uptake rate set at 100%), the number of unknowns was reduced to nine (Appendix Table 2). Seven unknowns were estimated by assuming a known chemical composition, while the remaining two unknowns were derived from experimentally determined metabolic tracer ratios (eqs. (1) and (2)). We used v_{10} and v_{14} as the two remaining unknown reactions rates (Appendix Table 2), but other variable combinations can be used instead.

2.2.2. Atom mapping matrices

In order to trace individual C atoms across the metabolic network, we used atom mapping matrices (AMM; Zupke and Stephanopoulos, 1994). These matrices described for each reaction how individual C atoms were transferred from substrate to product. The AMMs were $m \times n$ matrices with n equal to the number of C atoms in the substrate (rows in AMM) and m the number of C atoms in the product (columns in AMM). For example, the atom mapping matrices for the reaction (v_{10}) $G6P \rightarrow RU5P + CO_2$ were:

$$[G6P \rightarrow RU5P] = \begin{bmatrix} 0 & 1 & 0 & 0 & 0 & 0 \\ 0 & 0 & 1 & 0 & 0 & 0 \\ 0 & 0 & 0 & 1 & 0 & 0 \\ 0 & 0 & 0 & 0 & 1 & 0 \\ 0 & 0 & 0 & 0 & 0 & 1 \end{bmatrix}, \quad (3)$$

and

$$[G6P \rightarrow CO_2] = \begin{bmatrix} 1 & 0 & 0 & 0 & 0 & 0 \end{bmatrix}. \quad (4)$$

These matrices indicated that C_1 of G6P was released as CO_2; C_2 of G6P ended up in position 1 of RU5P; etc. The atom mapping matrices for other reactions were given in Appendix Table 1.

2.2.3. Label identification vector

The label identification vector identified the ^{13}C-labeled atoms in reaction substrates and products. For example, glucose labeled in positions 1 and 6 is represented as:

$$1,6 - {}^{13}\text{C glucose} = \begin{bmatrix} 1 \\ 0 \\ 0 \\ 0 \\ 0 \\ 1 \end{bmatrix}. \tag{5}$$

For each reaction, the flux rate was multiplied with AMM and the label identification vector of the substrate, thus generating a new label identification vector for the reaction product, which was used in the next reaction. Equation (6) calculates how ^{13}C was transferred from G6P to RU5P in reaction v_{10} (with v_{10} as the rate of the reaction), as follows:

$$v_{10} \times \begin{bmatrix} 0 & 1 & 0 & 0 & 0 & 0 \\ 0 & 0 & 1 & 0 & 0 & 0 \\ 0 & 0 & 0 & 1 & 0 & 0 \\ 0 & 0 & 0 & 0 & 1 & 0 \\ 0 & 0 & 0 & 0 & 0 & 1 \end{bmatrix} \times \begin{bmatrix} 1 \\ 0 \\ 0 \\ 0 \\ 0 \\ 1 \end{bmatrix} = \begin{bmatrix} 0 \\ 0 \\ 0 \\ 0 \\ v_{10} \end{bmatrix}. \tag{6}$$

In this example, ^{13}C located in C_6 of $1,6$-^{13}C G6P ends up in C_5 of RU5P. Similarly, the ^{13}C located in C_1 of $1,6$-^{13}C G6P is transferred to CO_2 with a rate calculated as:

$$v_{10} \times \begin{bmatrix} 1 & 0 & 0 & 0 & 0 & 0 \end{bmatrix} \times \begin{bmatrix} 1 \\ 0 \\ 0 \\ 0 \\ 0 \\ 1 \end{bmatrix} = [v_{10}]. \tag{7}$$

The end-result of the calculation was used as the label identification vector for the next reaction, taking into account multiple sources and total flux rates. For F1,6P, produced from $1,6$-^{13}C G6P via pentose phosphate pathway shunt at a rate of $v_{12} + v_{13}$, and via glycolysis at a rate of v_2, this calculation is as follows:

$$\left(\begin{bmatrix} 0 \\ 0 \\ 0 \\ 0 \\ 0 \\ v_{12} \end{bmatrix} + \begin{bmatrix} 0 \\ 0 \\ 0 \\ 0 \\ 0 \\ v_{13} \end{bmatrix} + \begin{bmatrix} v_2 \\ 0 \\ 0 \\ 0 \\ 0 \\ v_2 \end{bmatrix} \right) \div (v_{12} + v_{13} + v_2)$$

$$= \begin{bmatrix} \frac{v_2}{v_{12} + v_{13} + v_2} \\ 0 \\ 0 \\ 0 \\ 0 \\ \frac{v_{12} + v_{13} + v_2}{v_{12} + v_{13} + v_2} \end{bmatrix} = \begin{bmatrix} \frac{v_2}{v_{12} + v_{13} + v_2} \\ 0 \\ 0 \\ 0 \\ 0 \\ 1 \end{bmatrix}. \tag{8}$$

Because oxaloacetate was produced and consumed by cyclic reactions, we used twelve spin-up calculations to arrive at the steady-state labeling pattern. These spin-up calculations represented twelve runs through the Krebs cycle under constant labeling and asymptotically approached the stable partial enrichment values to within 1% (data not shown).

In this paper, we used 1-^{13}C and $2,3$-^{13}C pyruvate and 1-^{13}C and U-^{13}C glucose as metabolic tracer pairs. These compounds had the following label identification vectors:

$$\begin{bmatrix} 1 \\ 0 \\ 0 \end{bmatrix}, \quad \begin{bmatrix} 0 \\ 1 \\ 1 \end{bmatrix}, \quad \begin{bmatrix} 1 \\ 0 \\ 0 \\ 0 \\ 0 \\ 0 \end{bmatrix} \quad \text{and} \quad \begin{bmatrix} 1 \\ 1 \\ 1 \\ 1 \\ 1 \\ 1 \end{bmatrix}.$$

2.2.4. Solving model equations

To constrain the model, we used the proportional precursor demand of the soil microbial community as input variables. The proportional precursor demand was the relative requirement for metabolic precursors feeding biosynthesis reactions v_{14}–v_{21}. The precursor demand was a function of the chemical composition of microbial cells, estimated from published values for fungi, gram-positive and gram-negative bacteria, and scaled up to the microbial community level using 1:1:1 as the relative abundance of these groups of organisms. The assumption of a constant proportional precursor demand was equal to assuming a constant biochemical composition of the microbial cells. The proportional precursor demand does not determine the rate of microbial growth in the model.

The known and constant proportional precursor demand reduced the stoichiometric model to a set of equations with two unknowns, which were determined from experimentally determined ratios of position-specific $^{13}CO_2$ production from the two metabolic tracers (eqs. (1) and (2)). The model equations were solved using 'Solver', a linear programming tool in Excel, by varying v_{10} and v_{14} reactions rates until the $^{13}CO_2$ production ratios (eqs. (1) and (2)) calculated by the model matched those observed experimentally, under condition that all fluxes were greater than or equal to zero in the direction of the arrows. The reaction rates (v_2–v_{21} normalized relative to v_1), isotopologue ratios, flux partitioning ratios, CUE, and energy production (Appendix Table 1) were calculated by the model.

Flux partitioning ratios at major metabolic branch points were calculated as follows:

$$\Phi 1 = \frac{v_2}{v_2 + v_{10}}, \tag{9}$$

as flux partitioning between glycolysis and pentose phosphate pathway.

$$\Phi 2 = \frac{v_{21}}{v_{21} + v_{11}}, \tag{10}$$

as flux partitioning between pentose biosynthesis and total pentose phosphate pathway activity.

$$\Phi 3 = \frac{v_9}{v_9 + v_5}, \tag{11}$$

as flux partitioning between pyruvate carboxylase and pyruvate dehydrogenase.

CUE was calculated as

$$\text{CUE} = \frac{6 \times v_1 - \sum CO_2}{6 \times v_1}. \tag{12}$$

ATP production was calculated using the flux rates and the energy produced per reaction (Appendix Table 1), assuming that NADPH and NADH produced 2.5 ATP and $FADH_2$ equaled 1.5 ATP (Nelson and Cox, 2008).
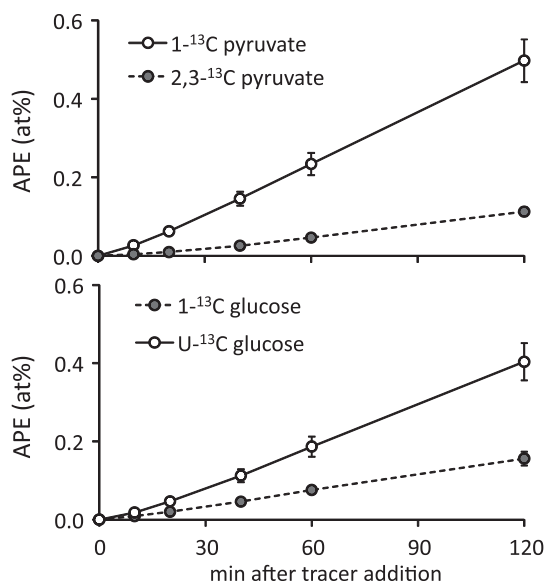
Fig. 2. Position-specific $^{13}CO_2$ production (and standard errors; expressed in atom percent excess) from pyruvate and glucose metabolic tracer isotopologues in a young volcanic soil (n = 8).

2.3. Sensitivity analysis

To evaluate the sensitivity of model to changes in proportional precursor requirement, we changed the value of each variable by +10% or −10%. After changing the value for a single variable, we then adjusted the reactions rates to match the observed $^{13}CO_2$ production ratios from pyruvate and glucose, which for this sensitivity analysis were set at 2.89 for $C_1/C_{2,3}$ of pyruvate and 2.59 for C_U/C_1 of glucose.

3. Results

3.1. Position-specific $^{13}CO_2$ production

Position-specific $^{13}CO_2$ production increased linearly between 0 and 120 min (Fig. 2). The $^{13}CO_2$ production rate from 1-^{13}C pyruvate was greater than from 2,3-^{13}C pyruvate, and greater from U-^{13}C glucose than from 1-^{13}C glucose. The $C_1/C_{2,3}$ ratio of $^{13}CO_2$ production from pyruvate was 4.4 (s.e. = 0.41; n = 8), while C_U/C_1 ratio from glucose was 2.6 (s.e. = 0.06; n = 8). Ratios were

determined from linear regression of position-specific $^{13}CO_2$ concentration against time after metabolic tracer addition. Lowest R^2 value for the eight individual regressions was 0.98 (1-^{13}C pyruvate), 0.95 (2,3-^{13}C pyruvate), and 0.99 (1-^{13}C and U-^{13}C glucose). The theoretical expectation for $^{13}CO_2$ production from these tracers in the absence of biosynthesis was 0.5 for pyruvate and 6.0 for glucose. The observed ratios were significantly different from these theoretical expectations ($P < 0.05$), indicating significant biosynthesis and C flux through the pentose phosphate pathway.

3.2. Proportional precursor demand and model sensitivity

For a quantitative interpretation of the ratios of position-dependent $^{13}CO_2$ production, we developed a model that calculated these ratios as a function of C flux rates through the central metabolic network (Fig. 1). This model contained information on the proportional demand of microbial cells for biosynthetic precursors (G6P, F1,6P, GAP, PYR, ACCO, αKG, OAA and RU5P). We estimated proportional precursor demand for three categories of microorganisms (fungi, gram-positive and gram-negative bacteria) using nine studies in which microbial chemical composition was determined (Table 1). These studies were all in-vitro experiments and may thus be biased towards fast-growing organisms and valid only for species that can be cultured. Gram-positive and gram-negative bacteria were very similar in their precursor requirements, while fungi had higher demand for G6P (Fig. 3).

We evaluated the sensitivity of the model to changes in proportional precursor demand by altering each value of $v_{14}-v_{21}$ by +10% or −10% (Fig. 4A). Reaction v_2 was most sensitive to a change in input variables, exhibiting both positive (+3.6% increase in reaction rate when relative pyruvate precursor demand was increased by 10%) and negative responses (−6.5% when relative acetyl-CoA precursor demand was increased by 10%). However, these changes were small compared to a 10% change in $C_1/C_{2,3}$ of pyruvate and C_U/C_1 of glucose ratios (Fig. 4B). Neither of these changes had a large effect on CUE and total ATP production (between +2% and −3% change).

3.3. Modeling metabolic flux patterns

The 21 model equations were solved with nine input variables. Seven input variables were estimated assuming a constant community proportional precursor demand from information in Fig. 3 (fixing $v_{15}-v_{21}$ proportional to v_{14}), assuming a microbial

Table 1
Estimates of proportional precursor demand (expressed as a fraction of total precursor demand) to build bacterial and fungal biomass. Estimates were from studies using single species in in-vitro experiments. Differences between fungal species on the one hand and the gram-positive and gram-negative species on the other hand were not significant, except for the requirement for G6P ($P < 0.05$). The metabolite pool of E4P was included with Ru5P, and that of PGA was included with GAP.

Species	Category	G6P	F1,6P	RU5P	GAP	PEP	PYR	ACCO	OAA	αKG	Reference
Escherichia coli	G⁻	0.016	0.005	0.096	0.124	0.040	0.216	0.286	0.136	0.082	(1)
Beijerinckia indica	G⁻	0.016	0.006	0.101	0.130	0.057	0.227	0.234	0.143	0.086	(2)
Ralstonia metallidurans	G⁻	0.030	0.008	0.072	0.124	0.055	0.217	0.211	0.147	0.136	(3)
Bacillus subtilis	G⁺	0.059		0.070	0.139	0.054	0.250	0.175	0.149	0.103	(4)
Corynebacterium glutamicum	G⁺	0.019	0.007	0.108	0.134	0.050	0.170	0.235	0.161	0.118	(5)
Bacillus clausii	G⁺	0.063	0.037	0.052	0.088	0.053	0.225	0.233	0.125	0.124	(6)
Penicillium chrysogenum	Fungus	0.087	0.023	0.081	0.137	0.040	0.176	0.178	0.175	0.102	(7)
Aspergillus oryzae	Fungus	0.167	0.016	0.058	0.092	0.055	0.132	0.234	0.071	0.176	(8)
Saccharomyces cerevisiae	Fungus	0.133		0.071	0.076	0.057	0.205	0.229	0.110	0.119	(9)

Abbreviations as in text and Fig. 1. References (1) Varma and Palsson, 1993; (2) Wu et al., 2005; (3) Ampe et al., 1997; (4) Dauner and Sauer, 2001; (5) Marx et al., 1996; (6) Christiansen et al., 2002; (7) Henriksen et al., 1996; (8) Pedersen et al., 1999; (9) Gombert et al., 2001.
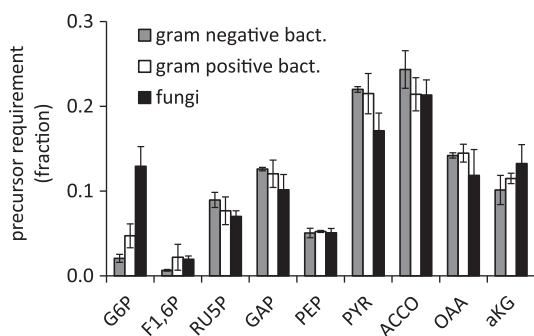
Fig. 3. Proportional precursor demand for bacterial (gram-positive, gram-negative) and fungal species (based on data in Table 1).

composition of fungi: gram-positive bacteria:gram-negative bacteria (F:B⁺:B⁻) ratio of 1:1:1. The remaining two unknowns were estimated using the experimentally determined $C_1/C_{2,3}$ $^{13}CO_2$ production ratio of pyruvate and C_U/C_1 ratio of glucose. Standard errors for modeled reaction rates were determined from the model results for each of the eight replicates. All fluxes were significantly different from zero (Fig. 5).

We determined the sensitivity of the model to community composition by comparing above results with modeled outcomes assuming contrasting community compositions: a bacteria-dominated (F:B⁺:B⁻ ratio of 1:4.5:4.5) and fungus-dominated (F:B⁺:B⁻ ratio of 8:1:1) community. Changes in overall proportional precursor demand associated with changed microbial community composition had only a modest effect on the individual flux rates (Table 2). Most fluxes were unaffected by changes in community composition, except for v_3 and v_4, which were significantly lower for fungi-dominated communities. The significant differences in biomass fluxes were the direct consequence of variation in input variables.

3.4. Estimating CUE, Φ1, Φ2, Φ3, and ATP production

The following modeling results were obtained using an F:B⁺:B⁻ ratio of 1:1:1. Based on the C flux pattern observed for this soil, we calculated CUE (0.72; s.e. 0.01). Carbon use efficiency was not significantly affected by changing the community composition (F:B⁺:B⁻ = 8:1:1 and 1:4.5:4.5; Table 2). Flux partitioning ratios at important branch points in the metabolic network were estimated as Φ1 = 0.67 (±0.04), Φ2 = 0.19 (±0.01) and Φ3 = 0.33 (±0.01). This indicated that 67% of all glucose-C taken up entered the pentose phosphate pathway, but only 19% of this was used for biosynthesis and 81% cycled back to glycolysis (while producing NADPH).Community composition did not significantly affect these estimates (data not shown).

Maximum ATP yield for 1 mol of glucose without biosynthesis was 3200 mol ATP per 100 mol glucose (Nelson and Cox, 2008). ATP production for this microbial community was 1080 mol ATP per 100 mol of glucose (±34) for the 1:1:1 = F:B⁻:B⁺ community. The energy production was slightly higher for bacteria (1088 ± 34 mol ATP) than fungi-dominated communities (1040 ± 34 mol ATP).

4. Discussion

Metabolic flux modeling is commonly applied to industrially important microbial strains and contributes to optimizing production of desirable products such as amino acids and antibiotics (e.g., Stephanopoulos, 1999). Although this is likely not
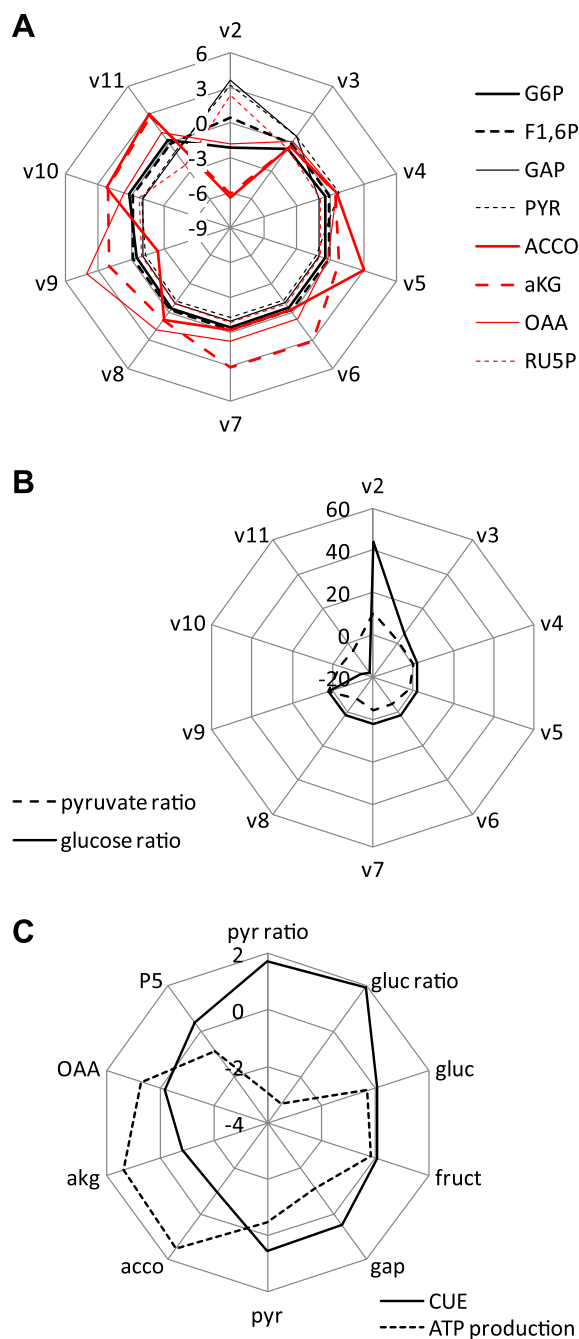
Fig. 4. Effects of 10% increases in proportional precursor demand for biosynthesis reactions (v_{14}–v_{21}) on reaction rates (v_2–v_{11}; A), 10% increase in $C_1/C_{2,3}$ ratio of pyruvate and C_U/C_1 ratio of glucose on reaction rates (% change relative to control; v_2–v_{11}; B), and 10% increases of pyruvate and glucose ratios and relative precursor demand on CUE and total ATP production (C). Some reactions of the pentose phosphate pathway (v_{12}–v_{13}) are not shown.

a goal for research on soils, a more complete understanding of soil biochemical processes may increase our understanding of the relationships between soil activity and microbial cell physiology and improve our ability to predict the effects of perturbations such as global climate change on soil CO_2 production and potential C sequestration. The paradigm of C and N control over soil activity (e.g., Allen and Schlesinger, 2004; Dijkstra et al., 2008; Hart et al., 1994) suggests that important changes in microbial physiology should occur when C or N becomes limiting.
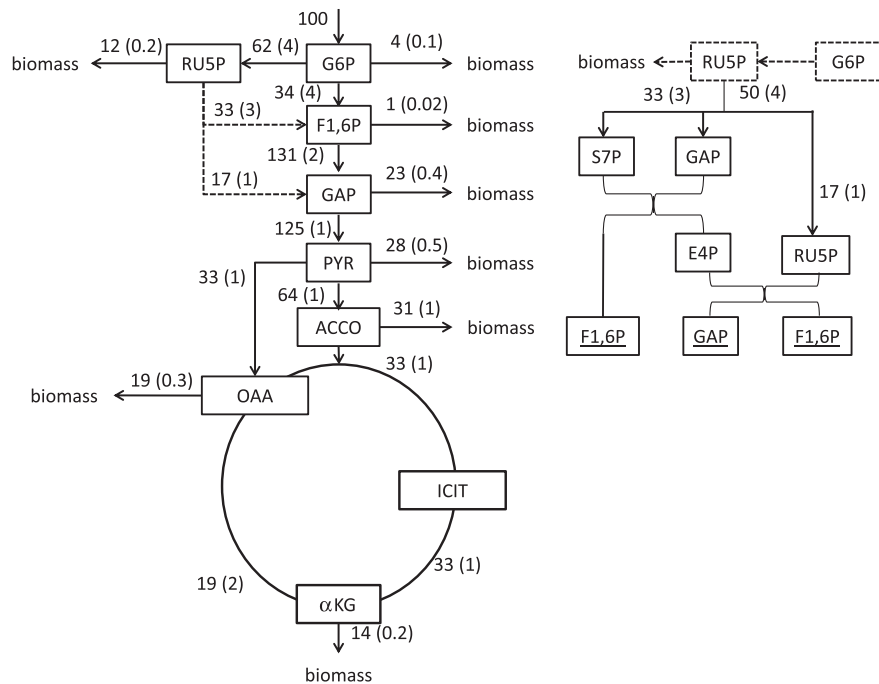
Fig. 5. Modeled rates (and standard error) for metabolic C fluxes in a young volcanic soil. Model assumes a $F:B^+:B^-$ ratio of 1:1:1.

These changes should be detectable using experimental and modeling approaches described in this paper. Similarly, CUE and partitioning of substrate-C over maintenance and growth processes are essential concepts widely used in soil and ecosystem models (Allison et al., 2010; Manzoni and Porporato, 2009). We can use this technique to determine these variables experimentally, without changing substrate availability. This could substantially aid in understanding soil processes. Changes in soil moisture content and C availability resulted in altered $C_1/C_{2,3}$ ratios for pyruvate and relative Krebs cycle activity (Dijkstra et al., 2011), as also noted for individual microbial species (Chen et al., 2009; Hua and Shimizu, 1999; Rühl et al., 2010). Similarities between biochemical response to environmental changes for single species and complex communities will increase our confidence in this analysis.

It is entirely possible that measurements of the details of soil metabolic systems will reveal little useful information. The soil is a relatively stable and buffered environment with respect to temperature and moisture, and changes in metabolic flux patterns may be rare or occur only in response to extreme perturbations. On the other hand, it is also possible that changes in metabolic flux patterns occur so rapidly and frequently that interpretation becomes meaningless. For example, Rühl et al. (2010) observed changes in flux patterns within 11 h accompanying a transition from C-excess to C-limited growth in a *Bacillus subtilis* culture. Future research will have to reveal whether persistent differences in microbial C flux patterns can be detected.

We have shown here that the measurement of C flux patterns in soil communities provides detailed information on metabolic reaction rates, which can be used to determine CUE, energy production for maintenance and growth processes, and be related to community-level measurements of soil respiration, oxygen consumption, and N mineralization. We are optimistic that this information will prove useful to soil scientists.

Table 2
Flux distributions (% relative to glucose uptake) and CUE for three hypothetical microbial communities with fungal:gram-positive bacteria:gram-negative bacteria = 1:1:1, 8:1:1, and 1:4.5:4.5. Abbreviations as in Fig. 1.

Flux	Community composition			P	Biomass flux	Community composition			P
	1:1:1	1:4.5:4.5	8:1:1			1:1:1	1:4.5:4.5	8:1:1	
v1	100	100	100	ns	v14	4.4	3.6	8.7	<0.05
v2	33.9	34.4	31.0	ns	v15	1.4	1.3	2.0	<0.05
v3	131.2	132.7	124.2	<0.05	v16	23.1	23.4	21.5	<0.05
v4	124.7	125.8	119.2	<0.05	v17	27.6	28.1	25.1	<0.05
v5	64.4	64.9	61.9	ns	v18	31.4	31.9	29.0	<0.05
v6	33.0	33.0	32.9	ns	v19	13.8	13.7	14.5	ns
v7	33.0	33.0	32.9	ns	v20	19.0	19.2	17.8	<0.05
v8	19.1	19.3	18.5	ns	v21	11.9	12.2	10.7	<0.05
v9	32.8	32.9	32.3	ns					
v10	61.7	62.0	60.3	ns	CUE	0.72	0.72	0.73	ns
v11	49.8	49.9	49.6	ns					
v13	33.2	33.2	33.1	ns					

4.1. Model assumptions

As most models, there are multiple assumptions in this model. The model assumes that glucose is the main microbial C source. Glucose and other carbohydrates are likely the dominant C substrates in surface soils, and derived from cellulose, hemicellulose, and starches. Glucose may not be the dominant substrate for microbes living deeper in the soil or in specialized niches where microbes decompose lignin or older soil organic matter into low molecular weight compounds such as acetate and succinate (Ornston and Stanier, 1966). Glucose may also not be the dominant C source in the rhizosphere where large amounts of organic acids are released (Dennis et al., 2010; Jones, 1998; Jones et al., 2003). Furthermore, anaerobic sites likely induce fermentation, producing compounds such as ethanol and lactate (Plassard and Fransson, 2009) that may be used as substrate in nearby aerobic sites. These compounds will rearrange the metabolic flux patterns and thereby influence the fate of the glucose and pyruvate tracers. For example, Schilling et al. (2007) found that glutamate utilization caused significant alterations of C fluxes over metabolic pathways. Similarly, Dijkstra et al. (2011) observed a strong reduction of $^{13}CO_2$ production from 1-^{13}C and 2,3-^{13}C pyruvate when succinate was added to soil. For these specialized niches, alternative models need to be developed.

We conclude that differences in chemical composition associated with microbial community composition have only a small effect on C flux patterns (Figs. 3 and 4; Table 2). However, the estimates of chemical composition were derived from *in-vitro* studies. It is clear that more information on the chemical composition and precursor demand is needed for microbes living in soils. For example, protein and RNA content increase at higher growth rates for some microbial species (Dauner and Sauer, 2001; Gombert et al., 2001), although not for *Escherichia coli* (Carlson and Srienc, 2004; Pramanik and Keasling, 1997). One way to determine the proportional precursor demand directly is to solve the model using a sufficiently large number of metabolic tracers. Our conclusion that microbial chemical and community composition does not change the model output much should not be interpreted to mean that community composition is not important for C flux patterns. A change in community composition can bring with it new metabolic capabilities that may alter substrate availability and utilization and potentially lead to large changes in metabolic flux patterns.

The model output variables showed only moderate sensitivity to changes in the proportional precursor demand, but high sensitivity to changes in $C_1/C_{2,3}$ ratio of pyruvate and C_U/C_1 ratio of glucose (Fig. 4). These results are encouraging, as they confirm that chemical composition of the microbes has limited influence, as also demonstrated by altering the $F:B^+:B^-$ ratios.

The model calculates the 'average community metabolic C flux pattern'. This C flux pattern is dominated by the most active and abundant species. Some of the less abundant species may exhibit different metabolic patterns, for example reductive or reverse Krebs cycle activity in certain autotrophic microbes (e.g., Buchannan and Arnon, 1990; Hügler et al., 2005), non-cyclic (or split) Krebs 'cycles' as in some primitive microbes and under anaerobic conditions (Meléndez-Hevia et al., 2008), and glyoxylate pathway and gluconeogenesis that may be activated when lipids or waxes are utilized (Gerstmeir et al., 2003). Although these alternative metabolic patterns are currently likely below the detection limit in bulk soil, they may be revealed when microsites are studied in isolation.

By comparing community flux patterns with flux patterns obtained for single species, we may gain some confidence that patterns observed in soil have biochemical relevance. For example, Φ1 (C partitioning over pentose phosphate pathway and glycolysis) in pure culture experiments ranged from 0.06 for *Saccharomyces cerevisiae* (Nissen et al., 1997) to 0.85 for *Phaffia rhodozyma* (Cannizzaro et al., 2004). We observed that in this soil almost 65% of C passes through the pentose phosphate pathway (Φ1), well within the range of values for single species. In general, higher values were obtained for aerobic than anaerobic conditions for single species (*S. cerevisiae*, *Torulopsis glabrata*, *Geobacillus thermoglucosidasius*, and *Corynebacterium glutamicum*; Gombert et al., 2001; Hua et al., 1999; Hua and Shimizu, 1999; Tang et al., 2007). A lower pentose phosphate pathway activity was observed for a microbial community in anaerobic soil compared with a nearby aerobic soil (T. Spada and P. Dijkstra, unpublished data). Likewise, the values we observed for Φ2 and Φ3 were within observed ranges for *in-vitro* experiments (e.g., Φ2 is 0.09–0.12 − Gombert et al., 2001 to 0.32–0.34 − Schilling et al., 2007; Φ3 is 0.12–0.28 − Schilling et al., 2007 to 0.74 − Nissen et al., 1997). Finally, CUE calculated using this model falls within the range of estimates by other researchers (0.32–0.77; Frey et al., 2001; Thiet et al., 2006 and references cited herein). We conclude, as did Thiet et al. (2006) and Six et al. (2006), that CUE does not vary with F:B ratio (Table 2). In contrast, CUE is affected by temperature (Allison et al., 2010; Steinweg et al., 2008), although this effect may be confounded with C availability (López-Urrutia and Morán, 2007; Manzoni et al., 2008, 2010). Carbon use efficiency is also negatively correlated with C:N ratio in litter (Manzoni et al., 2010), and is affected by grazing by protozoa (Frey et al., 2001), soil moisture content (Herron et al., 2009), glucose addition (Bremer and Kuikman, 1994; Shen and Bartha, 1996), C availability (Hart et al., 1994), and oxygen concentration (Parsons and Smith, 1989).

It is important to point out that additional position-specific ^{13}C-labeled metabolic tracer isotopologue pairs can be used to validate the model or guide further development. In fact, this model is already an improvement over a simpler model in which the pentose phosphate pathway is used for biosynthesis only without any recycling of C back to glycolysis (characterized as $v_{21} = v_{10}$; v_{11}, v_{12}, $v_{13} = 0$). The ratio of C_U/C_1 from glucose is greater than or equal to 6 when the pentose pathway shunt is inactive. C recycling via the pentose phosphate shunt is real because the actual measured value of C_U/C_1 from glucose was 2.61, significantly smaller than 6. Similarly, using additional tracer pairs, other aspects of the microbial metabolic network may be tested and improved.

Acknowledgements

Appendix

Appendix Table 1

Reaction stoichiometry, atom mapping matrices (following notation of Wiechert et al., 1997) and energy production. In many cases, the reaction is a sum over various reactions. For example, v_{10} represents the stoichiometry of three reactions: glucose-6P dehydrogenase, lactonase, and 6-phosphogluconate dehydrogenase. Biomass reactions (v_{14}–v_{21}) are not listed.

#	Reaction	AMM[a]	Energy production
v_1	Glucose → glucose-6P	abcdef → abcdef	−1 ATP
v_2	Glucose-6P → fructose-6P	abcdef → abcdef	
v_3	Fructose-6P → 2 glyceraldehyde-3P	abcdef → cba + def	−1 ATP
v_4	Glyceraldehyde-3P → pyruvate	abc → abc	+1 NADH + 2 ATP
v_5	Pyruvate → acetyl-CoA + CO_2	abc → bc + a	+1 NADH
v_6	Acetyl-CoA + oxaloacetate → isocitrate	ab + ABCD → abABCD	
v_7	Isocitrate → α-ketoglutarate + CO_2	abcdef → abdef + c	+1 NADPH
v_8	α-Ketoglutarate → oxaloacetate	abcde → abcd + e	+2NADH + ATP + FADH$_2$
v_9	Pyruvate + CO_2 → oxaloacetate	abc + A → abcA	−1 ATP
v_{10}	Glucose-6P → ribulose-5P + CO_2	abcdef → bcdef + a	+2 NADPH
v_{11}	2 Ribulose-5P → seduheptulose-7P + glyceraldehyde-3P	abcde + ABCDE → ABabcde + CDE	
v_{12}	Seduheptulose-7P + glyceraldehyde-3P → fructose-6P + erythrose-4P	abcdefg + ABC → abcABC + defg	
v_{13}	Ribuslose-5P + erythrose-4P → fructose-6P + glyceraldehyde-3P	abcde + ABCD → abABCD + cde	

[a] Letters identify position of C atoms in substrates and products.

Appendix Table 2

Reactions rates (Fig. 1) expressed relative to v_{10} and v_{14}. Coefficients (α_1–α_7) represent the proportional precursor demand relative to v_{14}. The right column represents equations using relative precursor demand for F:B$^+$:B$^-$ = 1:1:1.

Reactions	Reactions for F:B$^+$:B$^-$ = 1:1:1
$v_1 = 100$	100
$v_2 = v_1 - v_{10} - v_{14}$	$v_1 - v_{10} - v_{14}$
$v_3 = 2 (v_1 - (1/3)v_{10} - (1 + \alpha_1 + (2/3)\alpha_7)v_{14})$[a]	$2 (v_1 - 0.33v_{10} - 3.11v_{14})$[a]
$v_4 = 2v_1 - (1/3)v_{10} - (2 + 2\alpha_1 + \alpha_2 + (5/3)\alpha_7)v_{14}$	$2v_1 - 0.33v_{10} - 12.31v_{14}$
$v_5 = 2v_1 - (1/3)v_{10} - (2 + 2\alpha_1 + \alpha_2 + \alpha_3 + \alpha_5 + \alpha_6 + (5/3)\alpha_7)v_{14}$	$2v_1 - 0.33v_{10} - 25.98v_{14}$
$v_6 = 2v_1 - (1/3)v_{10} - (2 + 2\alpha_1 + \alpha_2 + \alpha_3 + \alpha_4 + \alpha_5 + \alpha_6 + (5/3)\alpha_7)v_{14}$	$2v_1 - 0.33v_{10} - 32.96v_{14}$
$v_7 = 2v_1 - (1/3)v_{10} - (2 + 2\alpha_1 + \alpha_2 + \alpha_3 + \alpha_4 + \alpha_5 + \alpha_6 + (5/3)\alpha_7)v_{14}$	$2v_1 - 0.33v_{10} - 32.96v_{14}$
$v_8 = 2v_1 - (1/3)v_{10} - (2 + 2\alpha_1 + \alpha_2 + \alpha_3 + \alpha_4 + 2\alpha_5 + \alpha_6 + (5/3)\alpha_7)v_{14}$	$2v_1 - 0.33v_{10} - 36.07v_{14}$
$v_9 = (\alpha_5 + \alpha_6)v_{14}$	$7.38v_{14}$
$v_{10} = v_{10}$	v_{10}
$v_{11} = v_{10} - \alpha_7 v_{14}$	$v_{10} - 2.68v_{14}$
$v_{14} = v_{14}$	$1.00v_{14}$
$v_{15} = \alpha_1 v_{14}$	$0.32v_{14}$
$v_{16} = \alpha_2 v_{14}$	$5.20v_{14}$
$v_{17} = \alpha_3 v_{14}$	$6.20v_{14}$
$v_{18} = \alpha_4 v_{14}$	$7.07v_{14}$
$v_{19} = \alpha_5 v_{14}$	$3.11v_{14}$
$v_{20} = \alpha_6 v_{14}$	$4.27v_{14}$
$v_{21} = \alpha_7 v_{14}$	$2.68v_{14}$

[a] v_3 is expressed in moles GAP relative to v_1, and thus twice as much as flux of fructose coming out of the F1,6P pool.

References

Allen, A.S., Schlesinger, W.H., 2004. Nutrient limitations to soil microbial biomass and activity in loblolly pine forests. Soil Biology and Biochemistry 36, 581–589.

Allison, S.D., Wallenstein, M.D., Bradford, M.A., 2010. Soil-carbon response to warming dependent on microbial physiology. Nature Geoscience 3, 336–340.

Ampe, F., Uribelarrea, J.-L., Aragao, G.M.F., Lindley, N.D., 1997. Benzoate degradation via the ortho pathway in Alcaligenes eutrophus is perturbed by succinate. Applied and Environmental Microbiology 63, 2765–2770.

Bremer, E., Kuikman, P., 1994. Microbial utilization of [14]C[U] glucose in soil is affected by the amount and timing of glucose additions. Soil Biology & Biochemistry 26, 511–517.

Buchannan, B.B., Arnon, D.I., 1990. A reverse Krebs cycle in photosynthesis: consensus at last. Photosynthesis Research 24, 47–53.

Cannizzaro, C., Christensen, N., Nielsen, J., von Stockar, U., 2004. Metabolic network analysis on Phaffia rhodozyma yeast using ^{13}C-labeled glucose and gas chromatography−mass spectrometry. Metabolic Engineering 6, 340–351.

Carlson, R., Srienc, F., 2004. Fundamental Escherichia coli biochemical pathways for biomass and energy production: identification of reactions. Biotechnology and Bioengineering 85, 1–19.

Chen, Z., Liu, H.-J., Zhang, J.-A., Liu, D.-H., 2009. Cell physiology and metabolic flux response of Klebsiella pneumonia to aerobic conditions. Process Biochemistry 44, 862–868.

Christiansen, T., Christensen, B., Nielsen, J., 2002. Metabolic network analysis of Bacillus clausii on minimal and semirich medium using 13C-labeled glucose. Metabolic Engineering 4, 159–169.

Dauner, M., Sauer, U., 2001. Stoichiometric growth model for riboflavin-producing Bacillus subtilis. Biotechnology and Bioengineering 76, 132–143.

Davidson, E.A., Janssens, I.A., 2006. Temperature sensitivity of soil carbon decomposition and feedbacks to climate change. Nature 440, 165–173.

Dennis, P.G., Miller, A.J., Hirsch, P.R., 2010. Are root exudates more important than other sources of rhizodeposits in structuring rhizosphere bacterial communities? FEMS Microbiology Ecology 72, 313–327.

Dijkstra, P., Blankinship, J.C., Selmants, P.C., Hart, S.C., Koch, G.W., Schwartz, E., Hungate, B.A., 2011. Probing C flux patterns of soil microbial metabolic networks using parallel position-specific tracer labeling. Soil Biology & Biochemistry 43, 126–132.

Dijkstra, P., LaViolette, C., Coyle, J.S., Doucett, R.R., Schwartz, E., Hart, S.C., Hungate, B.A., 2008. [15]N enrichment as an integrator of the effects of C and N on microbial metabolism and ecosystem function. Ecology Letters 11, 389–397.

Fernie, A.R., Geigenberger, P., Stitt, M., 2005. Flux an important, but neglected, component of functional genomics. Current Opinion in Plant Biology 8, 174–182.

Fischer, H., Kuzyakov, Y., 2010. Sorption, microbial uptake and decomposition of acetate in soil: transformations revealed by position-specific ^{14}C labeling. Soil Biology & Biochemistry 42, 186–192.

Frey, S.D., Gupta, V.V.S.R., Elliott, E.T., Paustian, K., 2001. Protozoan grazing affects estimates of carbon utilization efficiency of the soil microbial community. Soil Biology & Biochemistry 33, 1759–1768.

Gerstmeir, R., Wendisch, V.F., Schnicke, S., Ruan, H., Farwick, M., Reinscheid, D., Eikmanns, B.J., 2003. Acetate metabolism and its regulation in *Corynebacterium glutamicum*. Journal of Biotechnology 104, 99–122.

Gombert, A.K., Moreira dos Santos, M., Christensen, B., Nielsen, J., 2001. Network identification and flux quantification in the central metabolism of *Saccharomyces cerevisiae* under different conditions of glucose repression. Journal of Bacteriology 183, 1441–1451.

Hart, S.C., Nason, G.E., Myrold, D.D., Perry, D.A., 1994. Dynamics of gross nitrogen transformations in an old-growth forest: the carbon connection. Ecology 75, 880–891.

Haubensak, K.A., Hart, S.C., Stark, J.M., 2002. Influences of chloroform exposure time and soil water content on C and N release in forest soils. Soil Biology & Biochemistry 34, 1549–1562.

Henriksen, C.M., Christensen, L.H., Nielsen, J., Villadsen, J., 1996. Growth energetics and metabolic fluxes in continuous cultures of *Penicillium chrysogenum*. Journal of Biotechnology 45, 149–164.

Herron, P.M., Stark, J.M., Holt, C., Hooker, T., Cardon, Z.G., 2009. Microbial growth efficiencies across a soil moisture gradient assessed using ^{13}C-acetic acid vapor and ^{15}N-ammonia gas. Soil Biology & Biochemistry 41, 1262–1269.

Hua, Q., Fu, P.-C., Yang, C., Shimizu, K., 1999. Microaerobic lysine fermentations and metabolic flux analysis. Biochemical Engineering Journal 2, 89–100.

Hua, Q., Shimizu, K., 1999. Effect of dissolved oxygen concentration on the intracellular flux distribution for pyruvate fermentation. Journal of Biotechnology 68, 135–147.

Hügler, M., Wirsen, C.O., Fuchs, G., Taylor, C.D., Sievert, S.M., 2005. Evidence for autotrophic CO_2 fixation via the reductive tricarboxylic acid cycle by members of the ε subdivision of proteobacteria. Journal of Bacteriology 187, 3020–3027.

Jones, D.L., 1998. Organic acids in the rhizosphere – a critical review. Plant and Soil 205, 25–44.

Jones, D.L., Dennis, P.G., Owen, A.G., van Hees, P.A.W., 2003. Organic acid behavior in soils – misconceptions and knowledge gaps. Plant and Soil 248, 31–41.

Kruger, N.J., Ratcliffe, R.G., 2009. Insights into plant metabolic networks from steady-state metabolic flux analysis. Biochemie 91, 697–702.

Kuzyakov, Y., 1997. Abbau von mit ^{14}C spezifischmarkiertenaminosäurenimboden und decarboxylierungalseiner der natürlichenneutralisationsmechanismen. (Decomposition of ^{14}C specifically labeled amino acids in soil and decarboxylation as a natural neutralisation mechanism). Archiv für Acker- und Pflanzenbau und Bodenkunde 41, 335–343.

López-Urrutia, A., Morán, X.A., 2007. Resource limitation of bacterial production distorts the temperature dependence of oceanic carbon cycling. Ecology 88, 817–822.

Manzoni, S., Jackson, R.B., Trofymow, J.A., Porporata, A., 2008. The global stoichiometry of litter nitrogen mineralization. Science 321, 684–686.

Manzoni, S., Porporato, A., 2009. Soil carbon and nitrogen mineralization: theory and models across scales. Soil Biology and Biochemistry 41, 1355–1379.

Manzoni, S., Trofymow, J.A., Jackson, R.B., Porporato, A., 2010. Stoichiometric controls on carbon, nitrogen and phosphorus dynamics in decomposing litter. Ecological Monographs 80, 89–106.

Marx, A., de Graaf, A.A., Wiechert, W., Eggeling, L., Sahm, H., 1996. Determination of the fluxes in the central metabolism of *Corynebacterium glutamicum* by nuclear magnetic resonance spectroscopy combined with metabolite balancing. Biotechnology and Bioengineering 49, 111–129.

Meléndez-Hevia, E., Montero-Gómez, N., Montero, F., 2008. From prebiotic chemistry to cellular metabolism – the chemical evolution of metabolism before Darwinian natural selection. Journal of Theoretical Biology 252, 505–519.

Näsholm, T., Huss-Danell, K., Högberg, P., 2001. Uptake of glycine by field grown wheat. New Phytologist 150, 59–63.

Nelson, D.L., Cox, M.M., 2008. Lehninger – Principles of Biochemistry, fifth ed. WH Freeman and Company, New York.

Nissen, T.L., Schulze, U., Nielsen, J., Villadsen, J., 1997. Flux distributions in anaerobic, glucose-limited continuous cultures of *Saccharomyces cerevisiae*. Microbiology 143, 203–218.

Ornston, L.N., Stanier, R.Y., 1966. The conversion of catechol and protocatechuate to β-ketoadipate by *Pseudomonas putida*. I. Biochemistry. The Journal of Biological Chemistry 241, 3776–3786.

Parsons, L.L., Smith, M.S., 1989. Microbial utilization of carbon-14-glucose in aerobic vs. anaerobic denitrifying soils. Soil Science of America Journal 53, 1082–1085.

Pedersen, H., Carlsen, M., Nielsen, J., 1999. Identification of enzymes and quantification of metabolic fluxes in the wild type and in a recombinant *Aspergillus oryzae* strain. Applied and Environmental Microbiology 65, 11–19.

Plassard, C., Fransson, P., 2009. Regulation of low-molecular weight organic acid production in fungi. Fungal Biology Reviews 23, 30–39.

Pramanik, J., Keasling, J.D., 1997. Stoichiometric model of *Escherichia coli* metabolism: incorporation of growth-rate dependent biomass composition and mechanistic energy requirements. Biotechnology and Bioengineering 56, 399–421.

Quek, L.-E., Wittmann, C., Nielsen, L.K., Kromer, J.O., 2009. OpenFLUX: efficient modeling software for ^{13}C-based metabolic flux analysis. Microbial Cell Factories 8, 25. doi:10.1186/1475-2859-8-25.

Rühl, M., Zamboni, N., Sauer, U., 2010. Dynamic flux responses in riboflavin over producing *Bacillus subtilis* to increasing glucose limitation in fed-batch culture. Biotechnology and Bioengineering 105, 795–804.

Schilling, O., Frick, O., Herzberg, C., Ehrenreich, A., Heinzle, E., Wittmann, C., Stülke, J., 2007. Transcriptional and metabolic responses of *Bacillus subtilis* to the availability of organic acids: transcription regulation is important but not sufficient to account for metabolic adaptation. Applied and Environmental Microbiology 73, 499–507.

Selmants, P.C., Hart, S.C., 2008. Substrate age and tree islands influence carbon and nitrogen dynamics across a retrogressive semiarid chronosequence. Global Biogeochemical Cycles 22. doi:10.1029/2007/GB003062.

Selmants, P.C., Hart, S.C., 2010. Phosphorus and soil development: does the Walker and Syers model apply to semiarid ecosystems? Ecology 91, 474–484.

Shen, J., Bartha, R., 1996. Metabolic efficiency and turnover of soil microbial communities in biodegradation tests. Applied and Environmental Microbiology 62, 2411–2415.

Six, J., Frey, S.D., Thiet, R.K., Batten, K.M., 2006. Bacterial and fungal contributions to carbon sequestration in agroecosystems. Soil Science Society of America Journal 70, 555–569.

Steinweg, J.M., Plante, A.F., Conant, R.T., Paul, E.A., Tanak, D.L., 2008. Patterns of substrate utilization during long-term incubations at different temperatures. Soil Biology & Biochemistry 40, 2722–2728.

Stephanopoulos, G., 1999. Metabolic fluxes and metabolic engineering. Metabolic Engineering 1, 1–11.

Suthers, P.F., Burgard, A.P., Dasika, M.S., Nowroozi, F., Van Dien, S., Keasling, J.D., Maranas, C.D., 2007. Metabolic flux elucidation for large-scale models using ^{13}C labeled isotopes. Metabolic Engineering 9, 387–405.

Tang, Y.J., Sapra, R., Joyner, D., Hazen, T.C., Myers, S., Reichmuth, D., Blanch, H., Keasling, J.D., 2007. Analysis of metabolic pathways and fluxes in a newly discovered thermophilic and ethanol-tolerant *Geobacillus* strain. Biotechnology and Bioengineering 102, 1377–1386.

Thiet, R.K., Frey, S.D., Six, J., 2006. Do growth efficiencies differ between soil microbial communities differing in fungal:bacterial ratio? Soil Biology and Biochemistry 38, 837–844.

Varma, A., Palsson, B.O., 1993. Metabolic capabilities of *Escherichia coli*. II. Optimal growth patterns. Journal of Theoretical Biology 165, 503–522.

Wiechert, W., Möllney, M., Petersen, S., de Graaf, A.A., 2001. A universal framework for ^{13}C metabolic flux analysis. Metabolic Engineering 3, 256–283.

Wiechert, W., Siefke, C., de Graaf, A.A., Marx, A., 1997. Bidirectional reaction steps in metabolic networks: II. Flux estimation and statistical analysis. Biotechnology and Bioengineering 55, 118–135.

Wu, J.-R., Son, J.H., Seo, H.-J., Kim, K.-H., Nam, Y.-K., Lee, J.-W., Kim, S.-K., 2005. Metabolic flux analysis of *Beijerinckia indica* for PS-7 production. Biotechnology and Bioprocess Engineering 10, 91–98.

Yang, T.H., Heinzle, E., Wittmann, C., 2005. Theoretical aspects of ^{13}C metabolic flux analysis with sole quantification of carbon dioxide labeling. Computational Biology and Chemistry 29, 121–133.

Zamboni, N., Sauer, U., 2009. Novel biological insights through metabolomics and ^{13}C-flux analysis. Current Opinion in Microbiology 12, 1–6.

Zupke, C., Stephanopoulos, G., 1994. Modeling of isotope distributions and intracellular fluxes in metabolic networks using atom mapping matrices. Biotechnology Progress 10, 489–498.